JTTEE 2:243-250

Behavior of Ni-Al Particles in Argon: Helium Plasma Jets

W.D. Swank, J.R. Fincke, and D.C. Haggard

To better understand the plasma spray coating process, an experimental study of the interaction between a subsonic thermal plasma jet and injected nickel-aluminum particles was performed. The velocity, temperature, and composition of the argon/helium gas flow field was mapped using an enthalpy probe/mass spectrometer system. The sprayed particle flow field was examined by simultaneously measuring the size, velocity, and temperature of individual particles. Particle and gas temperatures were compared at the nominal substrate stand-off distance and axially along the median particle trajectory. Temperature and velocity differences between the particle and the gas surrounding it are shown to vary substantially depending on the trajectory of the particles. On the median trajectory, the average particle is transferring heat and momentum back to the plasma by the time it reaches the substrate. Because the exchange of heat and momentum is highly dependent on the particle residence time in the core of the plasma, the condition of particles at the substrate can be optimized by controlling the particle trajectory through the plasma.

1. Introduction

PLASMA spraying can be divided into three separate but interrelated processes. They are the plasma generation, the plasma/particle interaction, and the formation of the coating. Ideally, the process uniformly prepares particles with a given velocity, temperature, molten fraction, and chemical composition. These particles are then impacted on a substrate to build up the coating, particle by particle. This experimental investigation addresses the interaction of the particles with the gas flow field and how they arrive at the substrate with a given velocity, temperature, etc. The condition of the particles at impact determines individual splat morphology and coating characteristics such as porosity (density), adhesion, strength, and residual stress[1-3].

The plasma gas flow field parameters of temperature, velocity, enthalpy, and specie concentration describe the environment that particles are subjected to upon injection. Temperatures in the plasma are too high for the application of traditional measurement techniques such as thermocouples and uncooled pitot tubes and often are not high enough for application of emission spectroscopy. Although sophisticated laser techniques have been developed and applied to these types of flow fields, they are expensive and require delicate, complicated equipment.[4-6] In many situations, the use of thermodynamic probes represents a robust, low-cost alternative. The enthalpy probe is generally considered to be a reliable diagnostic tool in the range from 2000 to 14000 K[7-9] and has been used in high-temperature flow field research since the 1960s. More recently, the enthalpy probe has been rediscovered and is enjoying wide application to a variety of thermal plasma processing problems.[10-13] The measurement system used here integrates a differentially pumped quadrapole mass spectrometer with a fully automated enthalpy probe.[14]

Particle size, velocity, temperature, and number density characterize the particle flow field. The particle diagnostic system used to measure these parameters integrates a laser Doppler velocimeter with a two-color particle temperature measurement and an absolute magnitude of scattered laser light particle size measurement.[15]

The gas flow field maps obtained in Ar/He thermal plasma jets have been overlaid with the particle flow field measurements. Particle/gas temperature and velocity differences are presented along with a comparison of how the environment of a particle following the median trajectory differs from that of one following the geometric center line of the torch. Results from the plasma spraying of Ni-Al powder, a common bond coating, are presented.

Key Words: diagnostics, enthalpy probe, mass spectrometer, Ni-Al particles, plasma jet

W.D. Swank, J.R. Fincke, and **D.C. Haggard,** Idaho National Engineering Laboratory, EG&G Idaho, Inc., P.O. Box 1625, Idaho Falls, Idaho, 83415-2200, USA.

2. Measurement Techniques

The velocity, temperature, and composition of the hot gas flow field was mapped with an enthalpy probe/mass spectrometer system. The particle flow field was characterized by simultaneously measuring particle velocity, temperature, size, and relative number density. Both measurement techniques are discussed elsewhere;[14,15] hence, only a brief description is included here.

2.1 *Enthalpy Probe/Mass Spectrometer System*

An enthalpy probe is a water-jacketed gas sampling and stagnation pressure probe, from which the enthalpy, temperature, and velocity of a hot flowing gas can be derived once the composition is known. Gas enthalpy is determined using a calorimetric method that depends heavily on a tare or difference measurement. Observations of the coolant temperature rise and flow rate are made while no gas flows through the inner diameter of the probe. Gas is then allowed to flow, and the same coolant measurements are repeated, together with measurements of the

gas mass flow rate and gas temperature at the probe exit. The rate of heat removal from the gas sample is thus given by the difference between the measured difference of cooling water inlet and outlet temperatures;

$$\dot{m}_g(h_{1g} - h_{2g}) = \dot{m}_{cw} C_p[(\Delta T_{cw})_{\text{gas flow}} - (\Delta T_{cw})_{\text{no gas flow}}] \quad [1]$$

where $\dot{m}_g$ is the gas sample mass flow rate; $\dot{m}_{cw}$ is the cooling water mass flow rate; h_{1g} is the unknown gas enthalpy at the probe entrance; h_{2g} is the gas enthalpy at the probe exit thermocouple; C_p is the cooling water specific heat; and ΔT_{cw} is the cooling water temperature rise. Provided the gas sample flow rate, $\dot{m}_g$, and the gas enthalpy, h_{2g}, at the probe exit are known, the unknown gas enthalpy, h_{1g}, at the probe tip can be calculated. The exit gas enthalpy is determined from the measured temperature at atmospheric pressure, and the gas sample flow rate is measured via a sonic orifice. While the probe is in the "no gas flow" mode of measurement, it behaves like a water-cooled pitot tube, and the stagnation pressure is determined at the probe tip. Then for low Mach numbers, the free stream velocity, V, of the hot gas may be calculated from:

$$V = \left[\frac{2}{\rho}\left(P_{stag} - P_{atm}\right)\right]^{1/2} \quad [2]$$

where ρ is the mixture density; P_{stag} is the stagnation pressure; and P_{atm} is the local atmospheric pressure.

Thermodynamic properties such as density and enthalpy are determined from a Gibbs free energy minimization calculation.[16] For input to this calculation, the gas composition is measured. This was accomplished by integrating the enthalpy probe with a mass spectrometer. During the gas flow phase of the measurement, a gas sample is bled off to a quadrapole mass spectrometer or residual gas analyzer (RGA). The RGA (Leybold-Heraeus Inficon Quadrex 100) is set up in a differentially pumped vacuum system. The sample line for the RGA branches off from the probe gas sample line and is evacuated with a roughing pump to a pressure of approximately 1 torr. This pressure is regulated with a controlled leak valve at the probe gas sample line tee and was chosen low enough for good response time, but high enough to prevent preferential pumping of different sized molecules. A second controlled leak is located very close to the quadrapole sensor and is adjusted to maintain the pressure in the sensor vacuum system at approximately 10^{-6} torr.

The probe itself is fabricated from three concentric tubes. The outer tube is copper and has an outside diameter of 4.8 mm. The inner most tube is also copper and has an inside diameter of 0.78 mm. Copper was chosen because of its high thermal conductivity and formability. The middle tube is stainless steel and is not a pressure or heat transfer boundary, but guides the cooling water to and from the tip of the probe. A new probe can be fabricated and placed in the probe body in less than 2 man-hours. Being relatively inexpensive, this instrument can be used in areas of a plasma that are at a temperature very close to its survivability limit.

Although the construction of the probe is relatively simple, the calibration of the entire enthalpy probe system is complex. The residual gas analyzer is the most difficult and critical portion of the system to calibrate. Calibration is accomplished using known mixtures of argon, helium, and air. The limitations of the mass spectrometer and the largest source of error reside in the resolution of its 8-bit digitizer. This resolution error is minimized by optimizing the operating voltage of the electron multiplier and by adjusting the individual mass channel electronic gains until a reasonable sensitivity is achieved. Optimizing the gain in this way results in an uncertainty of 10% in the air fraction measurement, when the air fraction is in the neighborhood of 0.2, and a similar uncertainty in the argon to helium ratio under the same conditions.

Using standard techniques,[17] the estimated 2σ (standard deviation) uncertainty in measured enthalpy is 5.3%, with the major source of error being the determination of the gas mass flow rate through the probe. This error stems primarily from the inaccuracy of the thermocouple temperature measurement up stream of the sonic orifice. The combination of a 10% uncertainty in properties and a 5.3% uncertainty in the measured enthalpy results in an acceptable 2σ uncertainty of 4.9% in temperature, because at high temperatures (>6000 K) moderate changes in the enthalpy of the gas mixture produce small changes in the gas temperature. The gas mixture density is the major source of error in the gas velocity uncertainty of 6.3%.

2.2 *Particle Diagnostic System*

The system developed for the simultaneous measurement of particle size, velocity, and temperature integrates a crossed beam laser Doppler velocimeter (LDV) with a scattered light particle size measurement and a high-speed two-color pyrometer.[15] Physically, the measurement system consists of two sets of optics, transmission and receiving, that are rigidly mounted with the laser to a translation table. Movement of the table results in precise positioning of the measurement volume relative to the plasma device. A spatial resolution of less than 1 mm^3 makes it possible to map the distribution of particle size, velocity, temperature, and relative number density in typical flow fields.

The two-color pyrometer system is calibrated against a standard tungsten ribbon lamp. To simulate the passage of particles through the measurement volume, the lamp is placed behind a chopper rotating at constant speed. Errors in the determination of particle temperature arise from uncertainties in the calibration coefficients, the gray body assumption, and random fluctuations in the ratio of signal voltages. In combination, these lead to an estimated one standard deviation of uncertainty in temperature of 125 K at 2500 K. Calibration of the particle size measurement system is performed against a Berglund-Liu vibrating orifice aerosol generator using methanol as the working fluid.[18] A cor-

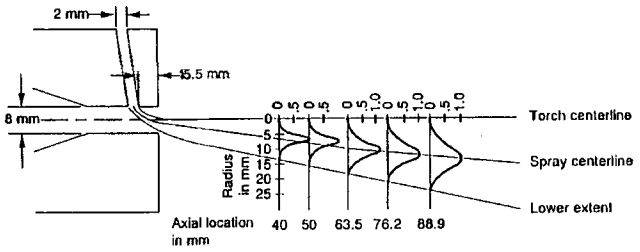

Fig. 1 Plasma torch geometry with normalized particle number density distribution.

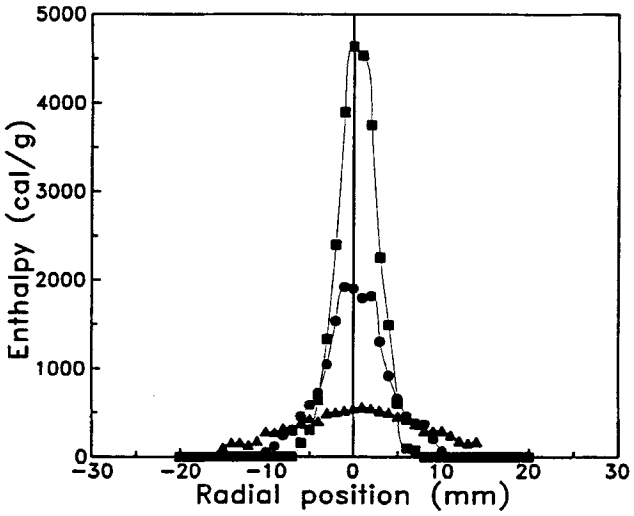

Fig. 2 Radial profiles of total enthalpy at axial positions of 5 (■), 30 (●), and 76.2 (▲) mm measured from the face of the torch.

rection to this calibration, based on Mie scattering theory and published values of the particle index of refraction, is then generated. The estimated one standard deviation uncertainty in size is 4.9 μm. In calibrating the laser Doppler velocimeter, only the laser wavelength and the angle between the beams is required to establish the relationship between the velocity of the scattering particle and the frequency output of the photodetector. The estimated velocity uncertainty is less than 5%.

3. Results and Discussion

Figure 1 shows the plasma torch geometry (Miller SG-100 with a 165/129 anode/cathode combination) and general particle flow field characteristics. Each of the particle number density curves shown is normalized to itself. For the chosen operating conditions, it is coincidental that the upper periphery of the sprayed particle flow field coincides with the centerline of the torch. Nominal torch operating conditions are 800 A at 35 V, for a total power input of 28 kW. At these conditions, the measured torch efficiency is 68%. The inlet plasma gas flow rate is 2830 L/h of argon and 1330 L/h of helium. The particle carrier gas flow rate is 368 L/h, also argon. All results were obtained in air at the local atmospheric pressure of 85.5 kPa.

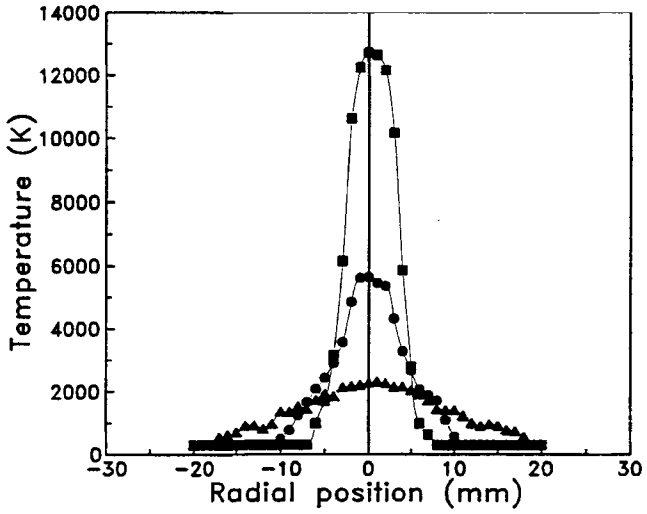

Fig. 3 Radial profiles of temperature at axial positions of 5 (■), 30 (●), and 76.2 (▲) mm measured from the face of the torch.

3.1 *Gas Flow Field*

The velocity, temperature, and composition of the gas flow field have been mapped between axial locations of 5 and 100 mm with the enthalpy probe. To prevent plugging of the probe, the enthalpy probe measurements were performed without particle injection, but include the effect of the particle carrier gas. This raises the question of particle loading effects on the plasma flow field.[19,20] At injection rates typical of industrial spraying conditions, the particle flow field is dilute in concentration ($<1000\ cm^{-3}$) and volume fraction ($<3 \times 10^{-5}$). Even though the mass fraction of particles is significant (approximately 30%) compared to the mass flow rate of gas, the energy and momentum extracted from the plasma for particle heating, melting, and acceleration is less than 5% of the total available. Hence, the assumption is made that the gross characteristics of the gas flow field are unchanged by the presence of particles.

Profiles of measured enthalpy and corresponding temperature are shown in Fig. 2 and 3, respectively. At an axial location 5 mm from the face of the torch, the measured centerline temperature was approximately 12,700 K. Near the torch exit, the radial temperature gradients are steep, and the temperature drops off rapidly to 2000 K at the 5-mm radial location, which is just outside of the 4-mm nozzle exit radius. Gradients at the 30-mm axial location are more gradual, dropping off from approximately 5600 K on the center line to 2000 K again at the 5-mm radial location. This spreading of the gas temperature profiles is due to turbulent entrainment of laboratory air into the jet. A similar effect is observed in the radial profiles of axial velocity (Fig. 4).

3.2 *Particle Flow Field*

A commercially available powder (Alloys International AI-1037), consisting of a nickel core with a Ni-Al skin that is bonded without the use of an organic binder, was used for this study. These particles are 50 to 125 μm in diameter and are injected on the diameter of the anode inside the body of the torch. The measured particle injection velocity is 15.0 m/s with a

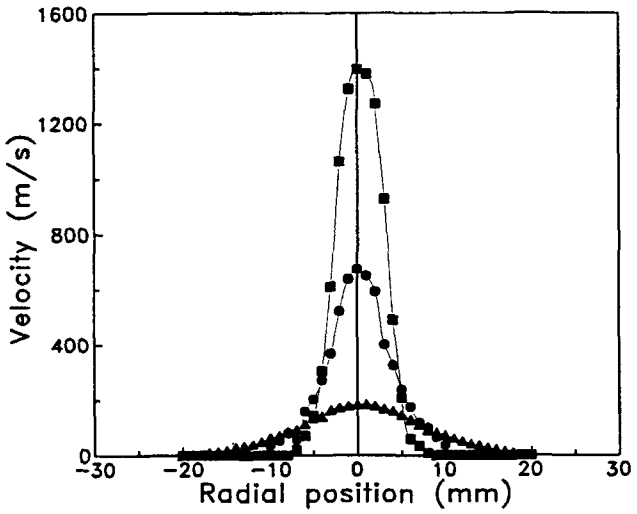

Fig. 4 Radial profiles of gas axial velocity at axial positions of 5 (■), 30 (●), and 76.2 (▲) mm measured from the face of the torch.

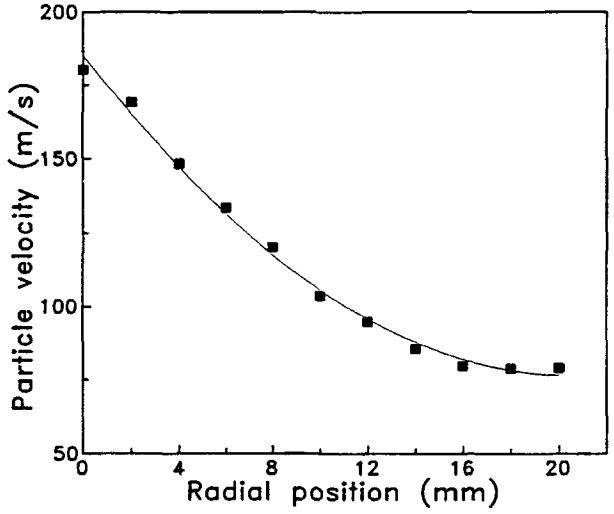

Fig. 6 Radial distribution of average particle axial velocity at an axial position of 63.5 mm measured from the face of the torch.

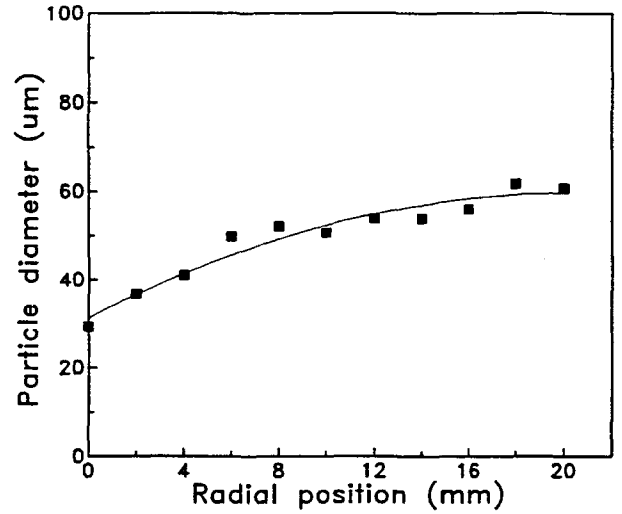

Fig. 5 Radial distribution of average particle size at an axial position 63.5 mm measured from the face of the torch.

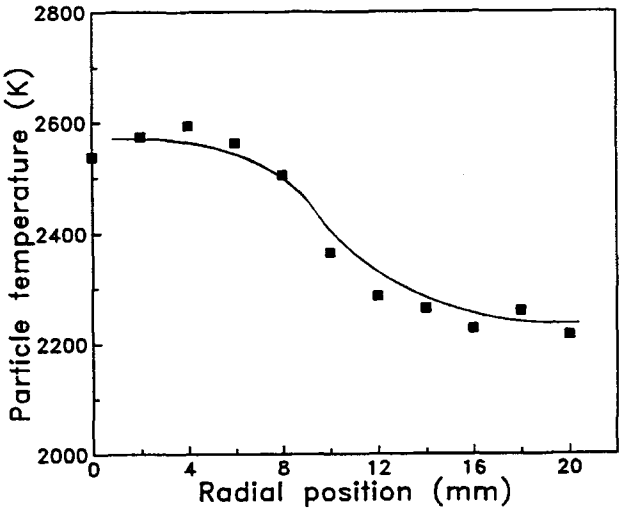

Fig. 7 Radial distribution of average particle temperature at an axial position of 63.5 mm measured from the face of the torch.

standard deviation of 2.4 m/s. Their initial momentum is transverse to the jet and large enough to cause the median particle trajectory to be below the geometric center line of the torch.

Particle parameters have been investigated between axial locations of 40 and 110 mm, and representative radial profiles of average particle size, velocity, and temperature appear in Fig. 5 through 7. In these figures, zero radial position is the geometric center line of the torch, and the particle injection is from left to right. The data shown are a complete scan across the plume, but due to the low particle number density on the injection side of the torch center line, no data were obtained (see Fig. 1). It is apparent that for the Ni-Al system there is significant flow/injection induced particle sizing, a pronounced tilt in the velocity profile, and a measurable tilt in the particle temperature distribution. The observed spatial distribution of size is consistent with intuition in that the larger, heavier particles appear farthest from the injection location. Measured particle temperatures are in excess of the 1900 K melting point of high nickel content Ni-Al alloys. Average particle velocities range from 180 m/s on the torch center line to 80 m/s in the periphery of the jet.

3.3 *Plasma-Spray Particle Interactions*

Particle measurements are necessarily Eulerian, i.e., a spatial description, hence, the history of an individual particle is known only in an average sense. By combining the particle and gas flow field measurements, the interactions between an average particle and the gas flow field can be examined. The environment that an average particle experiences is defined by the conditions on the median trajectory of the particle spray field. The median trajectory is defined as the path for which exactly one half the particles have trajectories lying above and below it. Figures 8, 9, and 10 are contour plots of the gas flow field temperature, veloc-

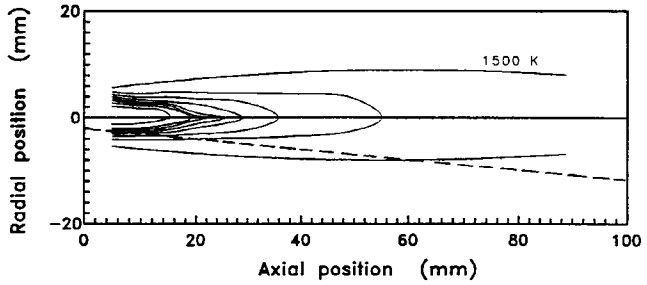

Fig. 8 Contour plot of gas temperature with the median particle trajectory shown by the dashed line. Contours are in increments of 1500 K.

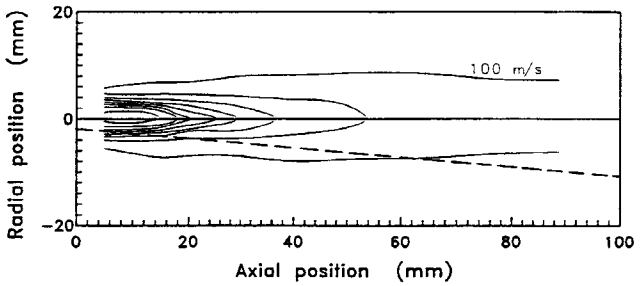

Fig. 9 Contour plot of gas axial velocity with the median particle trajectory shown by the dashed line. Contours are in increments of 200 m/s.

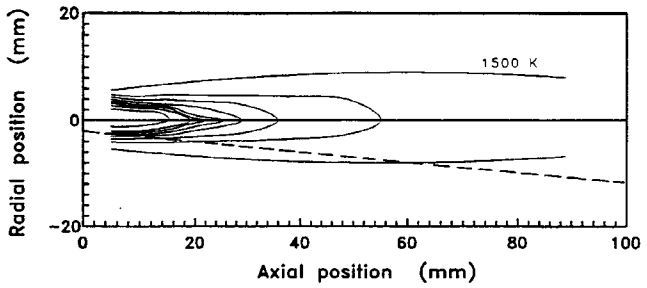

Fig. 10 Contour plot of air concentration with the median particle trajectory shown by the dashed line. Contours are in increments of 10%.

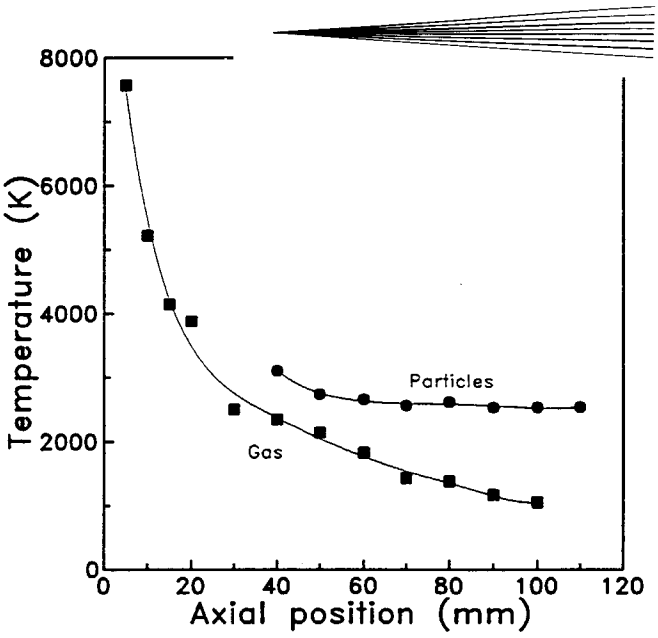

Fig. 11 Temperature of gas and particles on the median particle trajectory.

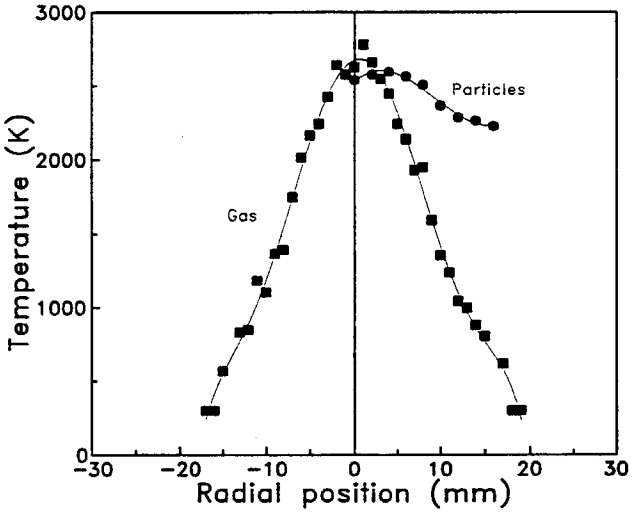

Fig. 12 Radial distribution of particle and gas temperature at the 63.5 mm axial position with "zero" radial position matching the geometric center line of the torch.

ity, and air concentration, respectively, with the dashed line indicating the median particle trajectory. The temperature map shows that the majority of particles exit the hottest portion of the plasma on the side opposite the point of injection. Particles traveling on the center line of the plasma plume do not see temperatures below 3000 K until the 55-mm axial position, and those traveling on the median trajectory of the particle flow field experience temperatures below 3000 K by the 20-mm axial position. Therefore, the average particle begins to transfer heat back to the gas sooner than if it followed the center line of the plasma. This is further illustrated in the plot of average particle temperature and the gas temperature along the median particle trajectory (Fig. 11). Noting that the absolute uncertainty is much larger than the point-to-point uncertainty in the data, the slight downward trend of average particle temperature is consistent with the trend of lower gas temperatures as one moves outward both axially and radially. A typical radial distribution of gas and particle temperature at an axial position of 63.5 mm is shown in Fig. 12.

Particles on the center line are generally hotter because they have been exposed to higher temperatures for a longer time and are smaller than those on the periphery of the spray field.

A similar scenario is observed in the measured velocities (Fig. 9). Although the 300 m/s contour extends to over 50 mm on the plasma center line, the average particle on the spray field center line experiences a gas velocity of less than 300 m/s by the 20-mm axial location. The cross over point of particle and gas axial velocities along the median trajectory of the particles is shown in Fig. 13. An average particle is accelerated by the gas, up to approximately 60 mm, and then afterward retarded by the surrounding gas. Typical radial profiles, at an axial position of 63.5 mm, of axial velocity for both the gas and particles is shown in Fig. 14. Again, due to their smaller size and longer exposure

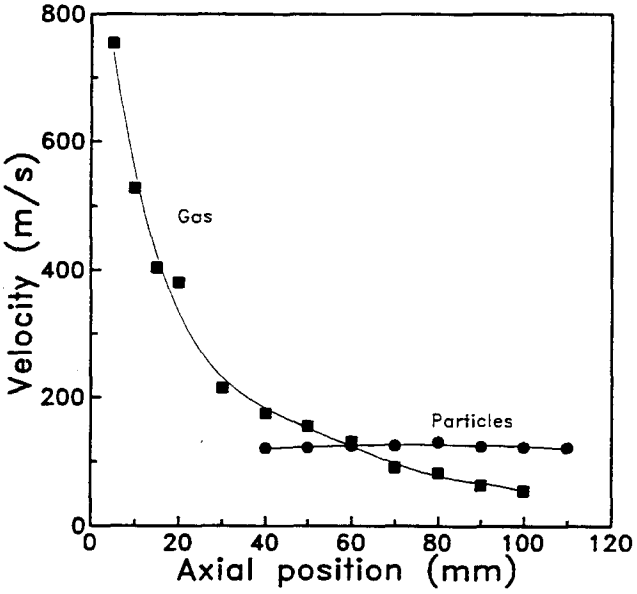

Fig. 13 Axial velocity of gas and particles along the median particle trajectory.

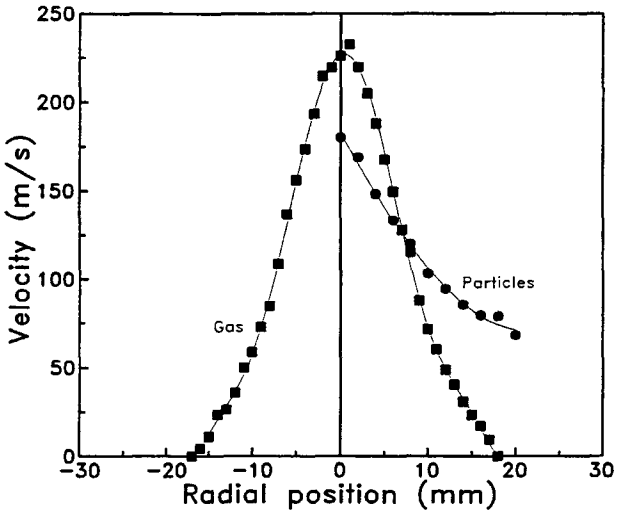

Fig. 14 Radial distribution of average particle and gas axial velocity at the 63.5 mm axial position with "zero" radial position matching the geometric center line of the torch.

to a higher velocity difference, the particles on the gas jet center line have a higher velocity than those in the periphery.

4. Conclusions

Complete maps of the gas flow field velocity, temperature, and specie concentration were made with an enthalpy probe. Without the intimidation of a costly probe tip, regions of the plasma jet with conditions that were very near the survival limit of this probe (approximately 14,000 K) were investigated. In-flight particle parameter data (particle size, velocity, temperature, and number density) in combination with maps of the gas flow field provided information on the environment that an average particle experiences as it travels to the substrate. Data of this type are useful in benchmarking and developing physically accurate models describing the spray coating process.[20]

Due to the asymmetry of the particle flow field, a particle traveling on the median trajectory experiences lower gas temperatures and accelerating forces than a particle that follows the center line of the plasma plume. By the time an average particle reaches the nominal substrate standoff, it is being cooled and decelerated by the plasma gas. Because the exchange of heat and momentum is dependent on the particles residence time in the core of the plasma, the condition, i.e., temperature, velocity, and molten fraction of particles at the substrate, can be optimized by controlling the particle trajectory through the plasma. Although not investigated here, it is generally possible to control the median trajectory of the particles by adjusting the carrier gas flow rate.

Acknowledgments

This work was supported by the U.S. Department of Energy, Assistant Secretary for Energy, Office of Basic Energy Sciences under DOE Contract No. DE-ACO7-76ID01570.

References

1. J. H. Zaat, A Quarter Century of Plasma Spraying, *Ann. Rev. Mater. Sci.*, Vol 13, 1983, p 9-42
2. J. M. Houben, Future Developments in Thermal Spraying, *Thermal Spray Coatings: New Materials, Processes and Applications*, F.N. Longo, Ed., Am. Soc. for Metals, 1984, p 1-19
3. H. Fukanuma, An Analysis of the Porosity Producing Mechanism, *Thermal Spray: International Advances in Coatings Technology*, C.C. Berndt, Ed., ASM International, 1992, p 767-772
4. S. C. Snyder et al., Determination of Gas-Temperature and Velocity Profiles in an Argon Thermal-Plasma Jet by Laser-Light Scattering, *Phys. Rev. E*, Vol 47 (No. 3), 1993, p 1996-2005
5. J.R. Fincke, R. Rodriguez, and C.G. Pentecost, Coherent Anti-Stokes Raman Spectroscopic Measurement of Air Entrainment in Argon Plasma Jets, *Plasma Processing and Synthesis of Materials III*, D. Apeilian and J. Szekely, Ed., Materials Research Society, Pittsburgh, 1990, p 184-191
6. J.R. Fincke, R. Rodriguez, and C.G. Pentecost, Measurement of Air Entrainment in Plasma Jets, *Thermal Spray Research and Applications*, T.F. Bernecki, Ed., ASM International, 1991, p 45-48
7. J. Grey, Thermodynamic Methods of High-Temperature Measurement, *ISA Trans.*, Vol 4 (No. 2), 1965, p 102-115
8. S. Katta, J.A. Lewis, and W.H. Galvin, A Plasma Calorimetric Probe, *Rev. Sci. Instr.*, Vol 44 (No. 10), 1973, p 1519-1523
9. J. Grey, P.F. Jacobs, and M.P. Sherman, Calorimetric Probe for the Measurement of Extremely High Temperatures, *Rev. Sci. Instr.*, Vol 33 (No. 7), 1962, p 738-741
10. J.R. Fincke, S.C. Snyder, and W.D. Swank, Comparison of Enthalpy Probe and Laser Light Scattering Measurement of Thermal Plasma Temperatures and Velocities, *Rev. Sci. Instr.*, Vol 64 (No. 23), 1993, p 711-718
11. W.L.T Chen, J. Heberlein, and E. Pfender, "Experimental Measurements of Plasma Properties for Miller SG-100 torch with Mach I Settings. Part 1: Enthalpy Probe Measurements," Engineering Research Center for Plasma-Aided Manufacturing, University of Minnesota, Aug 1990
12. M. Brossa and E. Pfender, Probe Measurements in Thermal Plasma Jets, *Plasma Chem. Plasma Process.*, Vol 8 (No. 1), 1988, p 75-90

13. A. Capetti and E. Pfender, Probe Measurements in Argon Plasma Jets Operated in Ambient Argon, *Plasma Chem. Plasma Process.*, Vol 9 (No. 2), 1989, p 329-341
14. W. D. Swank, J.R. Fincke, and D.C. Haggard, Modular Enthalpy Probe and Gas Analyzer for Thermal Plasma Measurements, *Rev. Sci. Instrum.*, Vol 64 (No. 1), 1993, p 56-62
15. J.R. Fincke, W.D. Swank, and C.L. Jeffery, Simultaneous Measurement of Particle Size, Temperature and Velocity in Thermal Plasmas, *IEEE Trans. Plasma Sci.*, Vol 18 (No. 6), 1990, p 948-957
16. S. Gordon and B. McBride, "Computer Program for Calculation of Complex Chemical Equilibrium Compositions, Rocket Performance, Incident and Reflected Shocks, and Chapman-Jouguet Detonations," NASA SP-273, Lewis Research Center, 1976
17. S.J. Kline and F.A. McClintock, Describing Uncertainties in Single-Sample Experiments, *Mech. Eng.*, 1953, p 3-9.
18. R.N. Berglund and B.Y.H. Liu, Generation of Monodisperse Aerosol Standards, *Env. Sci. Technol.*, Vol 7, 1973, p 147-152
19. A. Vardelle, M. Vardelle, P. Fauchais, P. Proulx, and M.I. Boulos, Loading Effect by Oxide Powders in DC Plasma Jets, *Thermal Spray: International Advances in Coatings Technology*, C.C. Berndt, Ed., ASM International, 1992, p 543-547
20. C.H. Chang, Numerical Simulation of Alumina Spraying in an Argon-Helium Plasma Jet, *Thermal Spray: International Advances in Coatings Technology*, C.C. Berndt, Ed., ASM International, 1992, p 793-798